Journal of Alloys and Compounds 788 (2019) 666–671

Contents lists available at ScienceDirect

Journal of Alloys and Compounds

journal homepage: http://www.elsevier.com/locate/jalcom

Molybdenum nanoparticles generation by pulsed laser ablation and effects of oxidation due to aging

Noe Zamora-Romero [a], Miguel A. Camacho-Lopez [b, *], Marco Camacho-Lopez [c], Alfredo R. Vilchis-Nestor [d], Victor H. Castrejon-Sanchez [e], Santiago Camacho-Lopez [f], Guillermo Aguilar [g]

[a] University of California, Riverside, Department of Materials Science and Engineering, 900 University Avenue, Riverside, CA 92521, United States
[b] Laboratorio de Fotomedicina, Biofotónica y Espectroscopía Láser de Pulsos Ultracortos, Facultad de Medicina, Universidad Autónoma del Estado de México, Jesús Carranza y Paseo Tollocan s/n, Toluca, 50180, Mexico
[c] Laboratorio de Investigación y Desarrollo de Materiales Avanzados, Facultad de Química, Universidad Autónoma del Estado de México, Campus Rosedal, Km 14.5 Carretera Toluca-Atlacomulco, Toluca, 50925, Mexico
[d] Centro Conjunto de Investigación en Química Sustentable, UAEM-UNAM, Facultad de Química, Universidad Autónoma del Estado de México, Toluca, 50120, Mexico
[e] Tecnologico de Estudios Superiores de Jocotitlan, Carretera Toluca Atlacomulco Km 44.8, Ejido San Juan y San Agustin, Jocotitlan, 50700, Mexico
[f] Centro de Investigación Científica y de Educación Superior de Ensenada, Carretera Ensenada-Tijuana, No. 3918, Zona Playitas, Ensenada B.C., 22860, Mexico
[g] University of California, Riverside, Department of Mechanical Engineering, 900 University Avenue, Riverside, CA 92521, United States

ARTICLE INFO

Article history:
Received 25 January 2019
Received in revised form
22 February 2019
Accepted 23 February 2019
Available online 25 February 2019

Keywords:
Molybdenum oxide
Aging process
Laser ablation
Nanoparticles oxidation
Core-shell
Picosecond pulses

ABSTRACT

Molybdenum oxides (MoO_x) nanoparticles (NPs) have great optical and electronic features that make them suitable for potential applications such as surface enhanced Raman spectroscopy (SERS) and energy systems. However, there are very few papers that report the synthesis of MoO_x NPs by using the laser ablation of solids in liquids (LASL) technique and they lack the explanation for the oxidation process. This work reports on the generation of NPs composed of molybdenum trioxide hydrated ($MoO_3 \cdot xH_2O$) ($x = 1$, 2) by using this method and its oxidation due to aging. A picosecond Nd:YAG laser was used and the per pulse laser fluence was varied from 5 to 20 J/cm^2. Spherical NPs were obtained with average diameters from 48 to 141 nm, respectively. The absorption evolution of the obtained colloids was characterized by optical absorption spectroscopy, TEM was used to study the MoO_x NPs morphology, size and structure and Raman spectroscopy to determine the material chemical composition.

1. Introduction

The so-called LASL technique is an effective method to obtain nanostructures [1]. This method is promising since the NPs formed can be free of both surfactants and other ions that exist during chemical synthesis [2], and it differs from laser ablation in vacuum or gaseous environments since the liquid can help to control some of the parameters of fabrication and to obtain the desired morphology and microstructure [3]. In the LASL process, material is removed from the surface of a target in the form of plasma by the application of a high pulsed laser beam. Usually a target is submerged in a liquid and the laser is focused on the target through the transparent medium [4,5].

When using the LASL method with metals, there are two main formation mechanisms proposed for the generation of nanostructures: i) the thermal evaporation with liquid interaction, and ii) the explosive ejection of nanodroplets. In the former, the formation of nanostructures is associated with the combination of ultrafast quenching of hot plasma and its interaction with surrounding media [6]. In the latter case, it is suggested that the laser irradiation could cause a local melting from the metal target, the adjacent liquid layer is heated to vapor or plasma state with a high pressure, which splashes the molten target into nanodroplets that react with the liquid medium and create the final nanostructures [7].

* Corresponding author.
E-mail addresses: mikentoh@hotmail.com, macamachol@uaemex.mx (M.A. Camacho-Lopez).

https://doi.org/10.1016/j.jallcom.2019.02.270
0925-8388/

On the other hand, one of the oxides that has attracted the attention of several groups are MoO_x [8–23], especially molybdenum trioxide (MoO_3), this is due to the potential applications as gas-sensing element [8,9], catalysts [10,11], in smart window devices [12] and as photothermal therapy agent for ablation of cancer cells [13,14]. MoO_x have several stoichiometries, ranging from full stoichiometric MoO_3, to more conducting reduced oxides in the form of MoO_{3-x} ($0 < x < 1$) and eventually semi-metallic MoO_2 [15,16].

The two most common crystal phases of MoO_3, are the thermodynamically stable orthorhombic α-phase and metastable monoclinic β-phase both are constructed in different ways, based on the MoO_6 octahedron building block [17–20]. These oxides are some of the most functional both optically and electronically due to their unique characteristics [21]. However, in spite of all their potential applications, we have only found three studies so far which include the generation of MoO_x NPs by using the LASL method [22–24].

In one study [22], binary oxides nanoparticles were synthesized by using the LASL method, using water or hydrogen peroxide-based coating liquid. Yellow MoO_3 and dark blue hydrated molybdic pentoxide ($Mo_2O_5 \cdot xH_2O$) nano-suspensions were obtained by irradiating with a Nd:YAG laser (1064 nm, 95 mJ per pulse) a Mo target. The average size of the MoO_3 NPs was about 8 nm, slightly larger than the $Mo_2O_5 \cdot xH_2O$ at 6.2 nm.

Another study [23] reported the generation of MoO_x NPs with average size of 100 nm by using a 20 ns laser at 510.6 and 578.2 nm with 9–10 W for 3 h at 10–12 kHz. The analysis of the structure and the composition of the colloid suspensions with an X-ray diffractometer shows evidence of MoO_3, MoO_2 and Mo NPs. Finally in Ref. [24], oblong and spherical MoO_x NPs with dimensions in the 20-100 nm range were obtained by using an external field-assisted ps laser at 532 nm, 100 kHz for 30 min. Evidence of α-MoO_3 was shown and they observed that there is no cell toxicity when using MoO_x NPs that were synthesized in DI water and ambient conditions.

However, there are several unanswered questions concerning the formation of the MoO_x NPs, especially the ones related to the post laser exposure aging process. For instance, the three studies fail to report either the time in which the spectroscopy studies were carried out or when the TEM micrographs were taken with respect to the date of NPs synthesis, which clearly plays an important role on the oxide formation or evolution, as the present study shows.

2. Experimental

2.1. Synthesis of the Mo NPs colloidal suspensions

We used a ps Nd:YAG (Ekspla, Lithuania) pulsed laser to irradiate a highly pure (99.95%) Mo target disk (*Kurt J, Lesker Co*) submerged in DI water which forms a 1 cm height column, at room temperature with no especial ambient conditions. The laser repetition rate, and the ablation time were kept constant. The laser beam was focused by using a convex lens (Fig. 1) of 200 mm focal length.

The Mo target was rotating while irradiating in order to avoid irradiation on the same target spot. The laser wavelength was at the fundamental 1064 nm, the pulse duration 30 ps, at a 10 Hz repetition rate, and per pulse laser fluence of 5, 10, 15 and 20 J/cm^2 for an exposure time of 5 min.

2.2. Sample characterization

2.2.1. UV–vis characterization

The optical characterization of the obtained colloidal suspensions was performed using a double beam spectrometer (Lambda 650 Perkin-Elmer) in the 200–900 nm range. For this purpose a quartz cuvette with an optical path length of 10 mm was used. The optical absorption spectra were taken on a regular basis right after the NPs synthesis and then for several weeks. All the experiments were performed under normal ambient conditions.

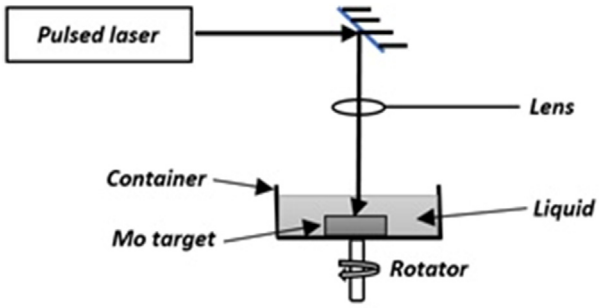

Fig. 1. LASL experimental set up. Picosecond laser pulses were used to ablate a Mo target submerged in DI water.

2.2.2. Transmission electron microscopy

TEM studies were carried out using a JEOL 2100 microscope operating at 120 kV accelerating voltage with a LaB_6 filament. The samples were prepared by placing drops of the NPs suspension over carbon-coated Cu grids, it was allow to evaporate, then observed in the TEM. In order to obtain information of the particle size, the length of many particles were measured employing ImageJ™ software. Particle size diameters were calculated with the equation $d_{avg} = \Sigma (n_i d_i)/\Sigma n_i$, where n_i is the number of particles of diameter d_i.

2.2.3. Raman spectroscopy

Raman spectroscopy was used to determine the crystalline structure of MoO_x NPs. Raman spectra were recorded using a micro-Raman Horiba Jobin Yvon system, model Xplora plus. A Solid-state laser ($\lambda = 532$ nm) was used to induce scattering with a nominal power of 25 mW. The laser beam was focused using a 100× lens and also it serves to recollect scattered light. The laser power on sample's surface was 1% of nominal power. A 1200 lines/mm grating was employed, 100 acquisitions were averaged with an exposure time of 1 s each one.

3. Results and discussion

3.1. Absorption spectrum of Mo NPs

Fig. 2 shows the absorbance of colloidal suspensions in DI water obtained right after irradiation with different energy fluences from 5 to 20 J/cm^2. The absorbance of DI water is also shown (black squares) as reference. We expected the value of the absorbance to be increased as the irradiation fluence was augmented due to fact that the absorbance is function of NPs concentration and size, and also the generation of larger NPs when irradiating with higher fluences [25]. It can be seen that the absorbance values obtained for 10 (blue upward triangles), 15 (green downward triangles) and 20 J/cm^2 (pink sideward triangles) behave as predicted, but is not the case for 5 J/cm^2 (red circles), since its value is higher than ones obtained for fluences of 10 and 15 J/cm^2. This occurs because the colloidal suspension obtained is more concentrated than the ones obtained with 10 and 15 J/cm^2.

Additionally, the absorbance spectra show a well-defined peak and a shoulder, which can clearly be seen in Fig. 2, at around 210 nm, and 240 nm, respectively. This is the characteristic

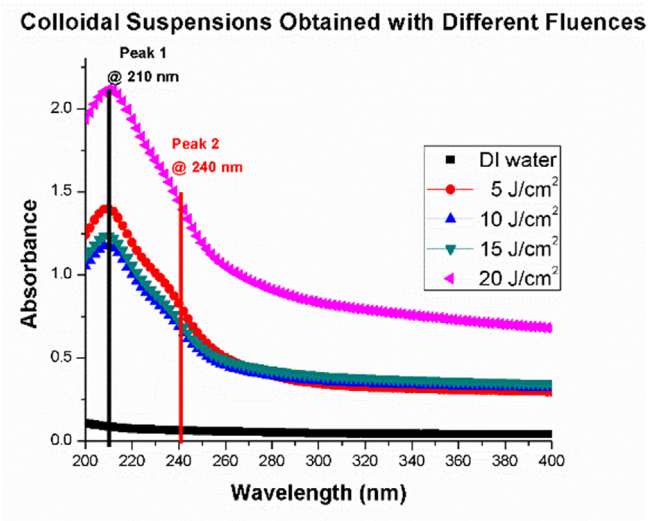

Fig. 2. MoO_x colloidal suspensions absorbance just after irradiation.

absorbance spectrum for spherical Mo NPs [26]. Noble and transition plasmonic metal NPs show similar absorbance spectra [27,28]. Different sizes of MoO_x NPs have been synthesized by using different synthesis methods that exhibit surface plasmonic resonance peaks in different spectral regions from UV to NIR, [29–31].

Fig. 3 shows a typical absorbance spectra time evolution of an aging colloidal suspension, which was obtained when irradiating the target with per pulse laser fluence of 5 J/cm^2. It shows that the absorbance increases as the colloidal suspension ages. Right after the ablation of the target, spherical Mo NPs are formed (red circles) according to its absorbance spectrum, which is known in the literature for such kind of Mo NPs with mean diameter tens of nm [26]. Once in the colloidal suspension, the Mo NPs interact with the surrounding water molecules of the liquid media, which starts surface oxidation of the NPs. This changes not only the metallic nature of the NPs but also its size and possibly its shape, getting as a result absorbance changes in time. At the end of the second week of aging the absorbance spectrum still shows its peak (vertical black line) at the same position, it is around 210 nm, the same applies for the shoulder (vertical red line) which remains at the 240 nm position, but a subtle shoulder appears around 320 nm.

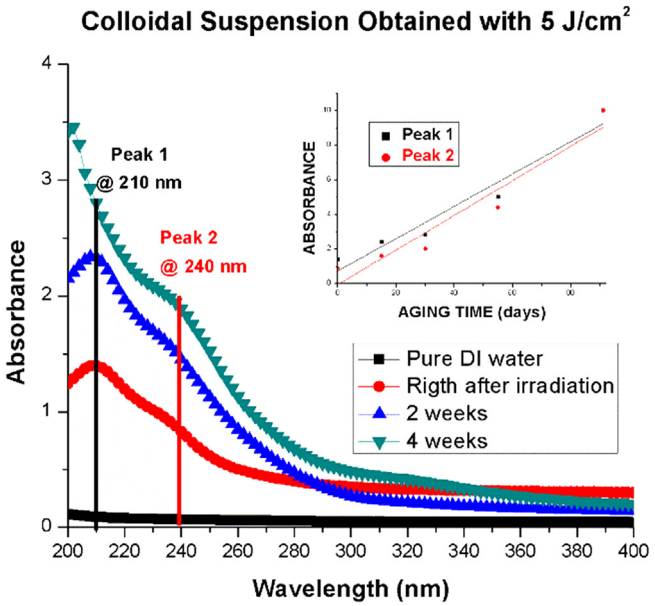

Fig. 3. MoO_x colloidal suspension absorbance evolution at different times.

At 4 weeks aging (green downward triangles) the NPs in the colloidal suspension are more oxidized and remarkably the peak in the absorbance spectrum shifts to shorter wavelength at around 200 nm, while the shoulders at 240 nm and 330 nm are enhanced; this spectrum shows features belonging to characteristic spherical MoO_3 NPs [26]. The inset shows the absorbance values for the peak and the shoulder as the colloidal suspension evolves in time. There is a linear increment of the absorbance as the suspension ages. We believe this can be explained by a growing layer of oxide around the Mo NP, giving place to the formation of a core-shell type structure [32].

3.2. TEM images of the MoO_x NPs

Fig. 4 shows typical images of the different types of NPs found three weeks after irradiation by using a TEM microscopy. As can be seen three types of nanoparticles are present: Mo NPs and MoO_x (a), Mo@MoO_x (b) and a Mo-MoO_x particle (c). The core of the nanoparticle appears darker because it is denser than the oxide layer that covers the Mo core, around the core the oxide shell has a light grey appearance. 4a) shows a large spherical Mo NP with a diameter in the order of 199 nm surrounded by a tiny MoO_x layer. Two small MoO_x NPs, are attached, one to the upper right and a second one at the bottom of the Mo NP, with diameters of 65 and 67 nm, respectively. In 4b) a medium size Mo NP can be seen with a diameter of 158 nm and a layer of MoO_x forming a MoO_x@Mo core-shell type of structure.

Finally, in 4c) there is quasi-spherical NP that seems to be formed by an agglomerate of several small nanoparticles, its diameter is around 135 nm and it has the thickest layer of MoO_x out of the three NPs shown. Notice a small MoO_x NP in the upper right, with a diameter of 35 nm.

With the help of the images obtained with the TEM microscope, we were able to identify three types of generated MoO_x NPs. Large (141 ± 12 nm) Mo NPs which are covered by a tiny molybdenum oxide layer, medium (97 ± 7 nm) sized NPs with a thicker layer of molybdenum oxide around a smaller core, and finally small (48 ± 4 nm) Mo NPs which form large quasi-spherical agglomerates. In the last case one can see abundant molybdenum oxide covering the agglomerate. In all three cases presented in Fig. 4, the core-shell type of structure is evident. Similar structures have been reported forming MoC@grafite NPs by using ps laser pulses [33].

By utilizing the TEM images, we measure the NPs diameter and plot the size distribution, Fig. 5. In 5 a), b) and c), it can be seen as expected that the average of the diameter of the MoO_x NPs increase as the energy of laser irradiation rises for 5, 10 and 15 J/cm^2 [25]. Actually, the average diameter of the NPs obtained with 10 and 15 J/cm^2 is almost twice and three times the size of the NPs generated with 5 J/cm^2, just like the augmentation of energy, respectively.

A Gaussian size distribution is appreciated in Fig. 5b and c), similar curve shapes have been reported for Ge [34] and Si [35] NPs synthesized with ps laser pulses. For d) 20 J/cm^2 the averaged diameter of the NPs does not follow the linear relation seen for lower energies and size. The average diameter of the NPs formed at this energy is smaller than the one obtained for 15 J/cm^2. This may occur because of the interaction of the beam with the large NPs, which causes its fragmentation [35].

3.3. Proposed mechanism of the Mo@MoOx NPs formation (aging effect)

A schematic hypothesis of the molybdenum oxidation process is

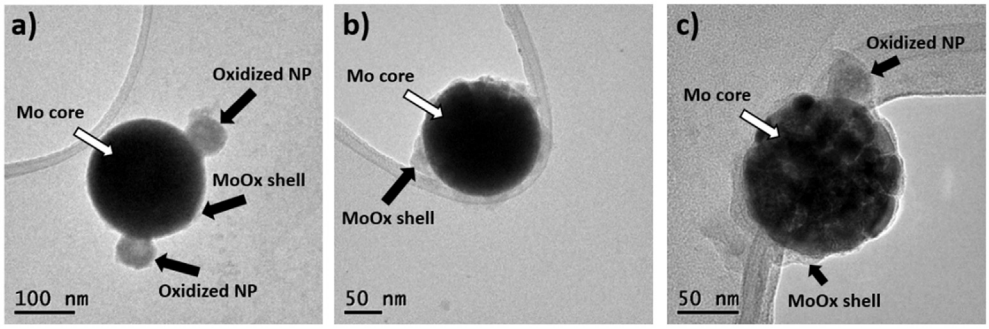

Fig. 4. TEM images of the MoO_x NPs.

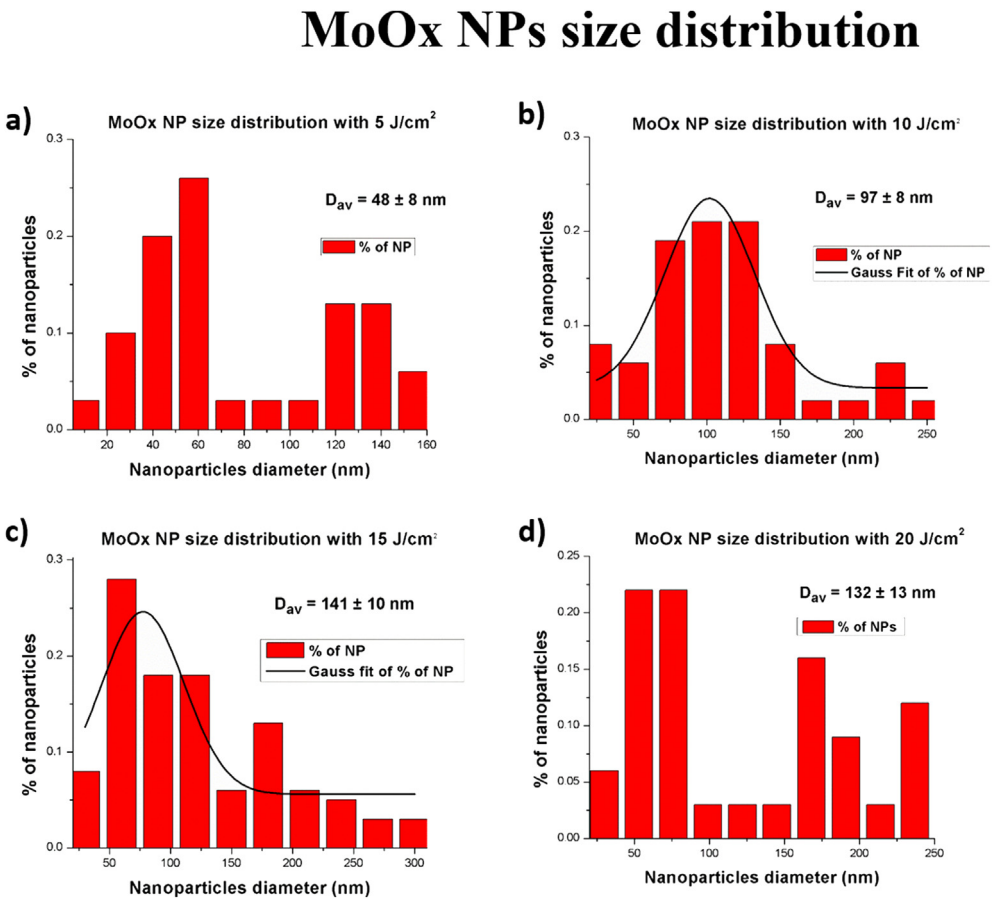

Fig. 5. Size distribution of the NPs obtained with a) 5 J/cm^2, b) 10 J/cm^2, c) 15 J/cm^2 and d) 20 J/cm^2.

shown in Fig. 6. Right after the formation of the Mo NPs, they interact with the liquid media. The water molecules oxidize the surface of the Mo NPs that have been created, as time passes the surface of the NPs keeps oxidizing since they are still submerged in the aqueous suspension; after several weeks the initial NPs evolve into either pure MoO_x or Mo@MoO_x in core-shell type NPs, this may depend on the initial size of the NP.

The NPs generated have diameters from tens to a few hundreds of nm. Fig. 6a) illustrates the aging process for large NPs; since large NPs are chemically more stable than medium and small ones due to the surface to volume ratio [36], they experience less oxidation and the average thickness of the oxide layer is smaller as compared to the one formed on medium and small NPs. For medium size NPs (Fig. 6b) the oxide layer is considerable thicker than the one found in large NPs. In the case of small NPs (Fig. 6c) right after been formed, two scenarios may take place due to their chemical instability. Some of the small NPs get attached to the surface of larger NPs, where they undergo oxidation; some others tend to form big agglomerates in order to achieve a more stable structure, still this agglomerate sees a considerable oxide layer formation.

3.4. Raman spectroscopy

The Raman spectrum in Fig. 7 shows different bands which are associated with molybdenum oxide hydrates ($MoO_3 \cdot xH_2O$) ($x = 1$, 2) [37]. These compounds structure come from the presence of MoO_5 (OH_2) octahedral sharing either corner equatorial oxygens or edges that exhibit different vibration modes. It can be seen two

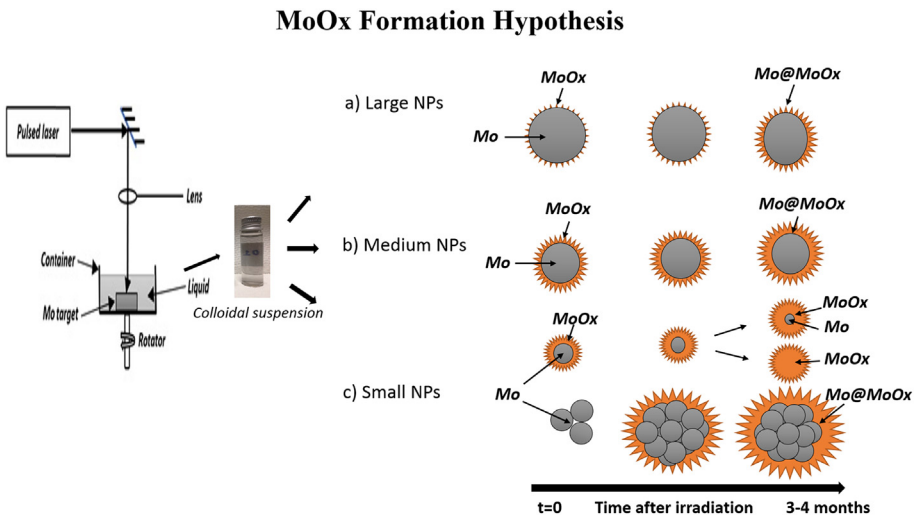

Fig. 6. MoO_x NPs colloidal suspension aging process hypothesis.

strong and broad bands, one at 245 cm^{-1} that can be assigned to deformation and lattice modes; and another at 974 cm^{-1} that can be assigned to stretching vibrations of νO=Mo, respectevely. A weak signal at 350 cm^{-1}, which is associated with $MoO_3 \cdot 2H_2O$ described as the νMo-OH_2 stretching vibrations. The band at 620 cm^{-1} is assigned to stretching vibrations of OMo_3 units that correspond to $MoO_3 \cdot H_2O$. Finally, at 865 cm^{-1} there is a small band that may be related to the bridging oxygens linked to two metal atoms in two dimensional arrangements corresponding to $MoO_3 \cdot 2H_2O$ [37].

4. Conclusions

This work presents the generation of spherical Mo@MoO_x NPs by using the LASL technique with potential application in energy systems or as photonic material. The average sizes are 48, 97, 141 and 132 nm obtained with laser fluences of 5, 10, 15 and 20 J/cm^2, respectively. The UV–Vis spectroscopy analysis showed that the colloidal suspension evolves in time, as a result of aging the absorbance increases. TEM images show the formation of three different types of NPs. Raman spectra shows that the NPs are composed of $MoO_3 \cdot xH_2O$, with $x = 1, 2$. Further studies are being conducted to synthesize MoO_x NPs that exhibit absorbance in the optical biological window in order to use them as potential photothermal agents.

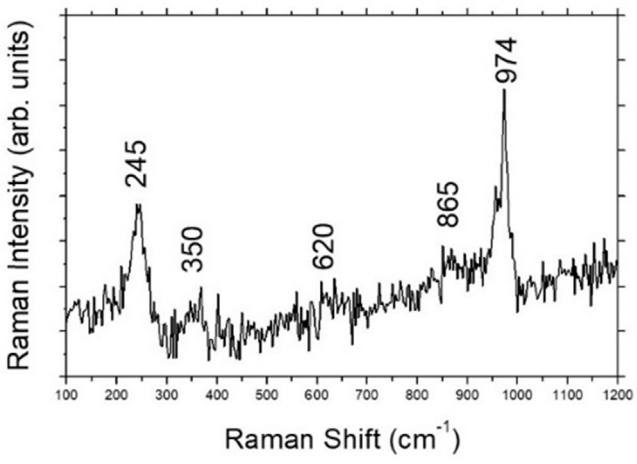

Fig. 7. Raman spectra of the hydrated molybdenum trioxide obtained.

Conflicts of interest

All authors claim not to have conflict of interest related to this article.

Acknowledgments

This work was possible thanks to the UCMEXUS-CONACyT scholarship for doctoral studies awarded to Noe Zamora-Romero. The financial support of CONACYT (Grant 280518) is gratefully acknowledged. This work was partially supported by SIEA-UAEM under the contract 4348/2017/CI.

Appendix A. Supplementary data

Supplementary data related to this article can be found at https://doi.org/10.1016/j.jallcom.2019.02.270.

References

[1] J. Dowden, The Theory of Laser Materials Processing, first ed., Springer series in materials science, 2008.
[2] A.V. Simakin, V.V. Voronov, G.A. Shafeev, Nanoparticle formation during laser ablation of solids in liquids, Phys. Wave Phenom. 15 (2007) 218. https://doi.org/10.3103/S1541308X07040024.
[3] S.I. Dolgaev, A.V. Simakin, V.V. Voronov, G.A. Shafeev, F. Bozon-Verduraz, Nanoparticles produced by laser ablation of solids in liquid environment, Appl. Surf. Sci. 186 (2002) 546. https://doi:10.1016/s0169-4332(01)00634-1.
[4] V. Amendola, M. Meneghetti, What controls the composition and the structure of nanomaterials generated by laser ablation in liquid solution? Phys. Chem. Chem. Phys. 15 (2013) 3027–3046. https://doi10.1039/C2CP42895D.
[5] H. Zeng, X.D. Du, S.C. Singh, S.A. Kulinich, S. Yang, J. He, W. Cai, Nanomaterials via laser ablation/irradiation in liquid: a review, Adv. Funct. Mater. 22 (2012) 1333–1353. https://doi:10.1002/adfm.201102295.
[6] P.S. Liu, W.P. Cai, H.B. Zeng, Fabrication and size-dependent optical properties of FeO nanoparticles induced by laser ablation in a liquid medium, J. Phys. Chem. C. 112 (9) (2008) 3261–3266. https://doi:10.1021/jp709714a.
[7] T.X. Phuoc, B.H. Howard, D.V. Martello, Y. Soong, M.K. Chu, Synthesis of $Mg(OH)_2$, MgO, and Mg nanoparticles using laser ablation of magnesium in water and solvents, Optic Laser. Eng. 46 (2008) 829–834. https://doi.org/10.1016/j.optlaseng.2008.05.018.
[8] M. Ferroni, V. Guidi, G. Martinelli, M. Sacerdoti, P. Nelli, G. Sbergveglieri, Characterization of a molybdenum oxide sputtered thin film as a gas sensor, Thin Solid Films 307 (1997) 148–151. https://doi.org/10.1016/S0040-6090(97)00279-4.

[9] Kim Won-Sik, Kim Hong-Chan, Hong Seong-Hyeon, Gas sensing properties of MoO_3 nanoparticles synthesized by solvothermal method, J. Nanopart. Res. 12 (2010) 1889–1896. https://doi:10.1007/s11051-009-9751-6.
[10] Y. Matsuoka, M. Niwa, Y. Murakami, Morphology of molybdenum supported on various oxides and its activity for methanol oxidation, J. Phys. Chem. 94 4 (1990) 1477–1482. https://doi:10.1021/j100367a051.
[11] J. Haber, H.E. Lalik, Catalytic properties of MoO_3 revisited, Catal. Today 33 (1993) 1–3, 119-137, https://doi:10.1016/S0920-5861(96)00107-1.
[12] J. Scarminio, A. Lourenco, A. Gorenstein, Electrochromism and photochromism in amorphous molybdenum oxide films, Thin Solid Films 302 (1997) 66–70. https://doi.org/10.1016/S0040-6090(96)09539-9.
[13] Y. Zhan, Y. Liu, H. Zu, Y. Guo, S. Wu, H. Yang, Z. Liu, B. Lei, J. Zhuang, X. Zhang, D. Huang, C. Hu, Phase-controlled synthesis of molybdenum oxide nanoparticles for surface enhanced Raman scattering and photothermal therapy, Nanoscale 10 (2018) 5997–6004. https://doi.org/10.1039/C8NR00413G.
[14] G.1 Song, J. Shen, F. Jiang, R. Hu, W. Li, L. An, R. Zou, Z. Chen, Z. Qin, J. Hu, Hydrophilic molybdenum oxide nanomaterials with controlled morphology and strong plasmonic absorption for photothermal ablation of cancer cells, ACS Appl. Mater. Interfaces 6 6 (2014) 3915–3922. https://doi:10.1021/am4050184.
[15] M. Cano-Lara, S. Camacho-López, A. Esparza-García, M.A. Camacho-López, Laser-induced molybdenum oxide formation by low energy (nJ)–high repetition rate (MHz) femtosecond pulses, Opt. Mater. 33 (2011) 1648–1653. https://doi.org/10.1016/j.optmat.2011.04.029.
[16] M.A. Camacho-López, L. Escobar-Alarcón, M. Picquart, R. Arroyo, G. Córdoba, E. Haro-Poniatowski, Micro-Raman study of the m-MoO2 to a-MoO3 transformation induced by cw-laser irradiation, Opt. Mater. 33 (2011) 480–484. https://doi.org/10.1016/j.optmat.2010.10.028.
[17] C. Julien, A. Mauger, A. Vijh, K. Zaghib, Lithium Batteries: Science and Technology, first ed., Springer International Publishing, 2016. https://doi.org/10.1007/978-3-319-19108-9.
[18] P.F. Carcia, E.M. McCarron III, Synthesis and properties of thin film polymorphs of molybdenum trioxide, Thin Solid Films 155 (1987) 53–63. https://doi.org/10.1016/0040-6090(87)90452-4.
[19] T. Pham, P. Nguyen, T. Vo, H. Nguyen, C. Luu, Facile method for synthesis of nanosized β–MoO_3 and their catalytic behavior for selective oxidation of methanol to formaldehyde, Adv. Nat. Sci. Nanosci. Nanotechnol. 6 (2015), 045010. https://doi:10.1088/2043-6262/6/4/045010.
[20] D.O. Scanlon, G.W. Watson, D.J. Payne, G.R. Atkinson, R.G. Egdell, D.S.L. Law, Theoretical and experimental study of the electronic structures of $MoO_3$and MoO_2, J. Phys. Chem. C 114 10 (2010) 4636–4645. https://doi:10.1021/jp9093172.
[21] I. Alves de Castro, R. Datta, J. Ou, A. Castellanos-Gomez, S. Sriram, T. Daeneke, K. Kalantar-zadeh, Molybdenum oxides – from fundamentals to functionality, Adv. Mater. 29 (2017) 1701619. https://doi:10.1002/adma.201701619.
[22] M. Maaza, B.D. Ngom, S. Khamlich, Valency control in MoO3−δ nanoparticles generated by pulsed laser liquid solid interaction, J. Nanopart. Res. 14 (2012) 714. https://doi.org/10.1007/s11051-011-0714-3.
[23] V.T. Karpukhin, M.M. Malikov, M.V. Protasov, T.I. Borodina, G.E. Val'yano, O.A. Gololobova, Composition, morphology characteristics, and optical properties of molybdenum oxide nanostructures synthesized by the laser ablation method in liquid, High Temp. 55 (2017) 870. https://doi.org/10.1134/S0018151X17060098.
[24] S. Spadaro1, M. Bonsignore, E. Fazio, F. Cimino, A. Speciale, D. Trombetta, F. Barreca, A. Saija, F. Neri, Molybdenum oxide nanocolloids prepared by an external shield-assisted laser ablation in water, EPJ Web Conf. 167 (2018), 04009. https://doi.org/10.1051/epjconf/201816704009.
[25] V. Amendola, M. Meneghetti, Laser ablation synthesis in solution and size manipulation of noble metal nanoparticles, Phys. Chem. Chem. Phys. 11 (2009) 3805–3821. https://doi.org/10.1039/B900654K.
[26] A. Ayi, Chinyere A. Anyama, K. Varsha, On the synthesis of molybdenum nanoparticles under reducing conditions in ionic liquids, J. Mater. (2015) 1–7, 372716, https://doi.org/10.1155/2015/372716.
[27] J. Shi, Y. Kuwahara, M. Wen, M. Navlani-García, K. Mori, T. An, H. Yamashita, Room-temperature and aqueous-phase synthesis of plasmonic molybdenum oxide nanoparticles for visible-light-enhanced hydrogen generation, Chem. Asian J. 00 (2016). https://doi:10.1002/asia.201600771.
[28] Jeffrey M. McMahon, wab George C. Schatza, Stephen K. Gray, Plasmonics in the ultraviolet with the poor metals Al, Ga, In, Sn, Tl, Pb, and Bi, Phys. Chem. Chem. Phys. 15 (2013) 5415–5423. https://doi10.1039/C3CP43856B.
[29] S.H. Lee, H. Nishi, T. Tatsuma, Tunable plasmon resonance of molybdenum oxide nanoparticles synthesized in non-aqueous media, Chem. Commun. 53 (2017) 12680–12683. https://doi10.1039/C7CC08090E.
[30] D. Ding, W. Guo, C. Guo, J. Sun, N. Zheng, F. Wang, M. Yan, S. Liu, MoO3-x quantum dots for photoacoustic imaging guided photothermal/photodynamic cancer treatment, Nanoscale 9 (2017) 2020–2029. https://doi10.1039/C6NR09046J.
[31] Y. Yang, Y. Yang, S. Chen, Q. Lu, L. Song, Y. Wei, X. Wang, Atomic-level molybdenum oxide nanorings with full-spectrum absorption and photoresponsive properties, Nat. Commun. 8 (2017) 1559. https://doi10.1038/s41467-017-00850-8.
[32] S. Dadashi, R. Poursalehi, H. Delavari, Optical and structural properties of Bi-based nanoparticles prepared via pulsed Nd:YAG laser ablation in organic liquids, Appl. Phys. A 124 (2018) 406. https://doi.org/10.1007/s00339-018-1817-9.
[33] M. Madrigal-Camacho, A.R. Vilchis-Nestor, M. Camacho-Lopez, M.A. Camacho-Lopez, Synthesis of MoC@Graphite NPs by short and ultra-short pulses laser ablation in toluene under N_2 atmosphere, Diam. Relat. Mater. 82 (2018) 63–69. https://doi.org/10.1016/j.diamond.2017.12.019.
[34] M. Rodio, A. Scarpellini, A. Diaspro, R. Intartaglia, Tailoring of size, emission and surface chemistry of germanium nanoparticles via liquid-phase picosecond laser ablation, J. Mater. Chem. C 5 (2017) 12264–12271. https://doi.org/10.1039/C7TC01992K.
[35] R. Intartaglia, K. Bagga, F. Brandi, Study on the productivity of silicon nanoparticles by picosecond laser ablation in water: towards gram per hour yield, Optic Express 22 (2014) 3117–3127. https://doi.org/10.1364/OE.22.003117.
[36] S. Eustis, M.A. El-Sayed, Why gold nanoparticles are more precious than pretty gold: noble metal surface plasmon resonance and its enhancement of the radiative and nonradioactive properties of nanocrystals of different shapes, Chem. Soc. Rev. 35 (2006) 209–217. https://doi.org/10.1039/B514191E.
[37] L. Seguin, Infrared and Raman spectra of MoO_3 molybdenum trioxides and $MoO_3 \cdot xH_2O$ molybdenum trioxides hydrates, Spectrochim. Acta 51 (1995) 1323–1344. https://doi.org/10.1016/0584-8539(94)00247-9.